

A SIMULATION STUDY OF BEAM PIPE EDDY CURRENT EFFECTS ON BEAM OPTICS

T. Asami*, The University of Tokyo, Tokyo, Japan
S. Igarashi, T. Koseki¹, Y. Kurimoto, Y. Sato, KEK, Ibaraki, Japan
¹also at The University of Tokyo, Tokyo, Japan

Abstract

In synchrotrons, fast changes of magnetic field induce eddy currents at the wall of beam pipes. The eddy currents cause a phase delay between excitation currents of the magnets and the magnetic field. The undesired magnetic field affected by eddy currents might be a serious obstacle in controlling beam optics precisely. In fact, in the operation of a high-intensity proton synchrotron J-PARC MR, the largest beam loss is observed at the beginning of acceleration when the magnetic field starts to vary in time. Therefore, it is important to estimate and understand the effects of eddy currents on beam optics. In this study, we have calculated the effect of eddy currents on magnetic field for some magnets in J-PARC MR, using electromagnetic simulation software. In this paper, we would like to report the details and results of the simulation.

INTRODUCTION

J-PARC MR is a high intensity proton synchrotron that accelerates protons from 3 GeV to 30 GeV. In Fast Extraction operation of MR, the repetition period will be shortened from 2.48 s to 1.32 s to achieve MW class intensity after 2022 by the upgrade of power supplies of magnets [1]. Due to the steeper acceleration pattern, larger eddy currents on the vacuum duct will be excited in the operation after the upgrade than those before the upgrade. Therefore, it is crucial to understand the effects of eddy currents in operation of MR with upgraded repetition cycle. In general, these effects of eddy currents can be measured by conducting the field measurement. However, for quadrupole magnets in MR, there are 13 types of beam ducts with different shapes and materials which will affect magnetic field differently. Since there are so many combinations of magnet shapes and duct types, conducting field measurement for all of them is difficult. On the other hand, it is necessary to understand the beam pipe eddy current effects on magnetic field after the MR upgrade for quadrupole magnets, since magnetic field error or undesired multipole fields in quadrupole magnets may cause such optics errors such as tune shifts and emittance growth which could lead to the beam loss directly. The purpose of this study is to calculate the effects of eddy currents on beam pipes using the electromagnetic simulation software CST Studio Suite [2] for quadrupole magnets. In this paper, the details of simulations done for quadrupole magnets are reported.

* tasami@post.j-parc.jp

SIMULATION STUDY FOR QUADRUPOLE MAGNETS

Quadrupole Magnets and Their Vacuum Ducts in MR

In MR, there are 216 quadrupole magnets which are driven by 11 different families of power supplies in respect to core length and focusing direction. Also, there are 13 types of vacuum ducts with different shapes and materials. Cross sections and materials of the vacuum ducts are shown in the Fig. 1. Note that the names of ducts shown in the figure are informal. Here, those ducts whose name starts with “Ti” or “UFO” are made of Titanium, and others are made of SUS316L. For magnets, even if their power supply family is the same, the duct shape might be different by their location depending on required physical aperture. Table 1 shows the number of magnets in MR for the combinations of power supply families and vacuum ducts. Here, the name of each family is expressed in three letters such as “QFR” and “QDT”, where the second letter “F” stands for focusing and “D” stands for defocusing in horizontal direction.

Simulation Model

In this study, three models with ducts “Ti130o”, “HAN-PEN” and “UFO140” were chosen for the simulation. Here, core shapes are identical in three models with longitudinal length of 1760 mm and bore radius of 70 mm (which corresponds to the magnets of QFR). Also, each model was constructed with precise dimensions and real materials of vacuum duct, end plates, side plates, coils, and core, including shimming shape at the core end. An example of simulation model is shown in Fig. 2. In the discussion below, the coordinate z is taken to be the longitudinal direction of the beam, and x and y to be the horizontal and vertical directions in the transverse plane respectively, as shown in Fig. 2. Mesh size was optimized so that the calculation errors of the B-field become less than 0.1% at the edge of good field region in the static magnetic field calculation. For quadrupole magnets in MR, the good field region is designed to be 65 mm radius circle whose center matches to the center of quadrupole magnet. The magnetic field at the edge of good field region was designed to be less than 0.05% in terms of relative error to the ideal magnetic field.

Here, GL value is defined as $G \equiv \frac{\partial B_y}{\partial x}|_{x=y=0}$ integrated along z -direction (hence, $\int G(z)dz$). Together with the beam momentum p and electric charge q , GL value gives the inversed value of focusing length of quadrupoles as $\frac{q}{p} \cdot GL$.

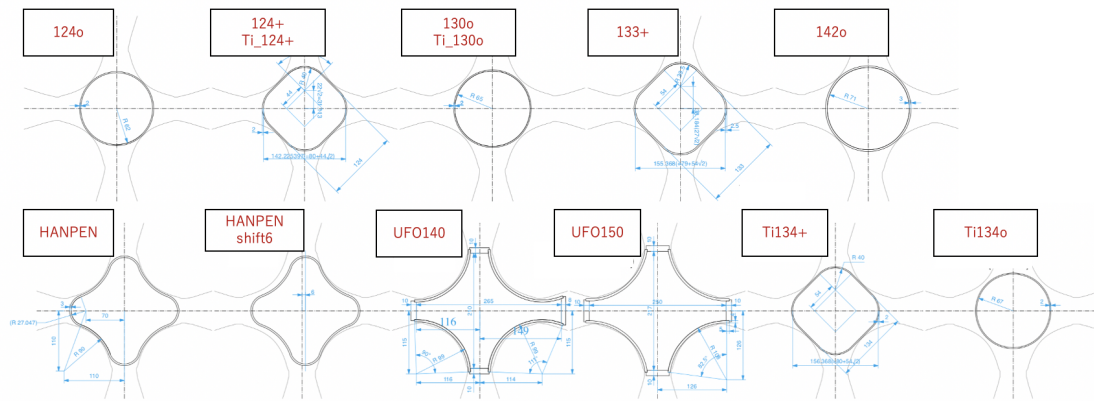


Figure 1: Vacuum ducts.

Table 1: Number of Quadrupole Magnets for Each Combinations of Power Supply Families and Vacuum Ducts

Duct Shape	Power Supply Families										
	QFP	QFX	QFS	QFT	QFN	QDX	QDS	QFR	QDN	QDR	QDT
124o	-	-	5	-	20	-	-	1	40	2	-
124+	-	-	-	-	20	22	-	1	-	2	-
130o	-	-	-	-	-	-	-	-	-	-	1
133+	4	-	-	4	-	-	5	1	-	-	1
142o	-	-	-	-	-	-	-	-	-	-	1
HANPEN	1	-	-	1	-	-	-	2	-	-	-
HANPENShift6	-	-	-	-	-	-	-	-	-	-	1
UFO140	-	-	-	-	-	-	-	1	-	-	-
UFO150	-	-	-	-	-	-	-	-	-	-	1
Ti134o	-	-	-	-	-	-	-	-	-	-	1
Ti134o	-	-	-	-	-	-	-	-	-	-	1
Ti134+	1	-	-	1	-	-	1	-	-	-	-
Ti130o	-	-	-	-	-	-	-	3	-	-	-
Ti124+	-	48	1	-	8	5	-	-	8	2	-

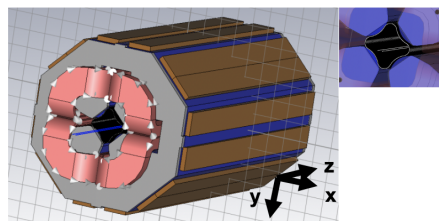


Figure 2: An example of simulation model.

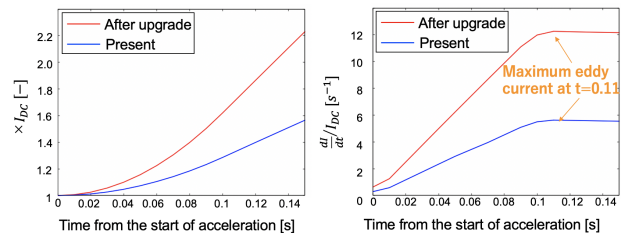


Figure 3: Input current patterns (left) and their derivatives $\frac{dI}{dt}$ (right).

Simulation Condition

In present operation of MR, the largest beam loss is observed at the beginning of acceleration when the magnetic field starts to vary in time. The repetition cycle upgrade will excite the larger eddy currents on the vacuum duct and might increase the beam loss at the beginning of acceleration. Therefore, we took start time of calculation to the start point of the acceleration, and duration to be 150 ms. Also, we have simulated for both coil current patterns for the present user operation and the high repetition rate operation after the upgrade of MR. These input coil current patterns are shown in the left of Fig. 3.

Below, we focused on the B-field at 110 ms from the start of the acceleration, where the eddy currents are the largest among each time step, as can be seen from the graph in the right of Fig. 3. From now on, field results at this timestamp will be shown.

B-Field in Quadrupole Magnet

For each of the simulation, the B-field for each of the three dimensional points in the model was calculated, and integrated along z-direction (“BL” value). Figure 4 shows the colormap of BL value plotted against each pair of x and y,

Content from this work may be used under the terms of the CC BY 3.0 licence (© 2021). Any distribution of this work must maintain attribution to the author(s), title of the work, publisher, and DOI

for the model with duct shape “HANPEN”. The dashed blue line is the good field region. The dashed red line is typical beam size at the corresponding actual magnet in MR. The beam size was evaluated from 2σ emittance [3] of the user operation and beta calculated by the beam optics simulation code SAD [4] at the actual location of corresponding magnet.

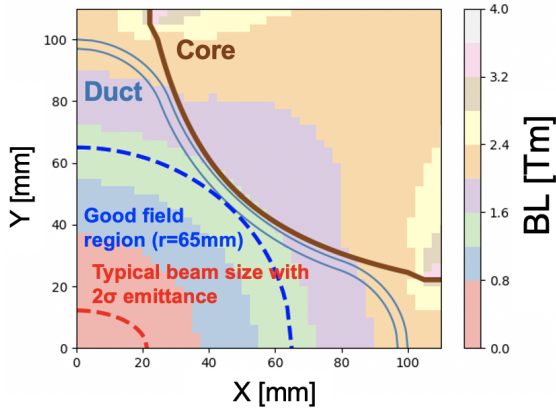


Figure 4: BL value plotted against each of the (x,y) at $t = 0.11$ s.

Quadrupole Field in the Present Pattern (2.48 s Cycle)

First, the input pattern was taken to be the present pattern with 2.48 s cycle. Figure 5 shows the y component of B-field integrated along z direction plotted against x, for the three types of ducts. The polynomial fit was conducted for each of the curve, and quadrupole components were derived from the coefficient of the first-degree component, which is exactly the GL value. The fitting was done for the good field region up to 5th order (hence, up to dodecapole component). The derived GL values are shown in Table 2.

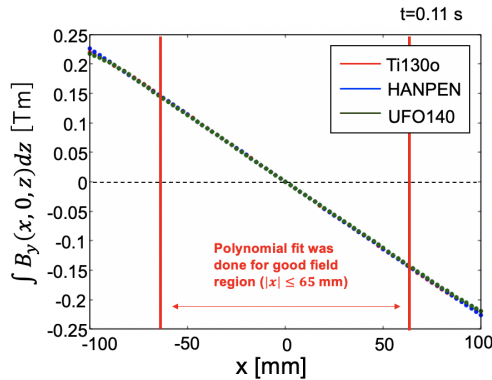


Figure 5: $f(x) \equiv \int B_y(x, 0, z)dz$ plotted against x .

The GL values of models for ducts Ti130o and HANPEN do match well. However, the difference between Ti130o or HANPEN and a model with UFO140 is significant. In relative error, the difference of the GL value for UFO140 from that of Ti130o can be estimated to be about 1%.

Table 2: GL Values for the Present Pattern Input

Duct Shape	GL [T]
Ti130o	2.2718 ±0.0023
HANPEN	2.2687 ±0.0023
UFO140	2.2502 ±0.0023

Quadrupole Field in High Repetition New Pattern (1.32 s Cycle)

The similar simulation was done with taking the input pattern to be the new pattern with the higher repetition operation. Again, the graph in the Fig. 6 shows the y component of B-field integrated along z direction plotted against x, for each model of the three types of ducts. The fitting was done in exactly the same manner as the simulation with present pattern. The derived GL values are shown in Table 3.

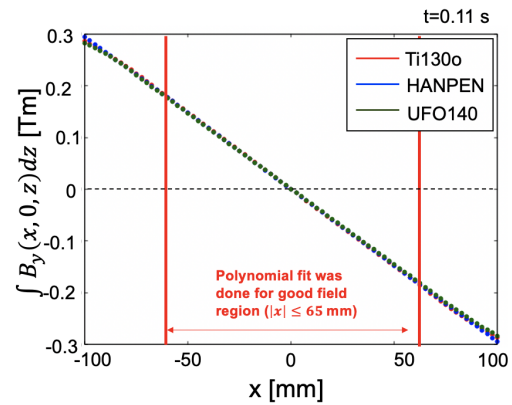


Figure 6: $f(x) \equiv \int B_y(x, 0, z)dz$ plotted against x .

Table 3: GL Values for the High Repetition New Pattern Input

Duct Shape	GL [T]
Ti130o	2.9556 ±0.0030
HANPEN	2.9498 ±0.0030
UFO140	2.9120 ±0.0030

Again, the difference of the GL value for UFO140 from Ti130o can be estimated to be about 1.5% in relative error.

CONCLUSION

We have calculated magnetic field error due to eddy currents on vacuum ducts for some quadrupole magnets in MR. In the calculation, it was shown that the difference in duct shape has been shown that it may affect at least about 1.5% to the field error for the high repetition rate operation. Now, we are planning a simulation study for all the models of quadrupole magnets in MR, and to evaluate effects on beam optics using tracking code.

REFERENCES

- [1] S. Igarashi, K. Satou, C. Ohmori, *et al.*, “Accelerator design for 1.3-MW beam power operation of the J-PARC Main Ring”, *Progress of Theoretical and Experimental Physics*, vol. 2021, no. 3, p. 033G01, Feb. 2021. doi:10.1093/ptep/ptab011
- [2] CST Studio Suite, https://www.aetjapan.com/software/CST_Overview.php
- [3] S. Igarashi *et al.*, “Study on the Beam Intensity Upgrade of J-PARC Main Ring”, in *Proc. of the 3rd J-PARC Symposium (J-PARC2019)*, Tsukuba, Japan, Sep. 2019, vol. 33, p. 011029. doi:10.7566/JPSCP.33.011029
- [4] SAD, <http://acc-physics.kek.jp/SAD/>.